Sandia National Laboratories, California
Thin-Film & Interface Research Program

Highlights 1997

Science of Metals

Alloy Theory

Advanced Ceramics

Interfacial Dislocation Dynamics

Influence of Dislocation Structure on Grain Boundary Dissociation

D.L. Medlin, G.H. Campbell, C.B. Carter

Motivation:

Recent work has shown that certain classes of grain boundaries form in a dissociated, three-dimensional configuration. In particular, Σ=3 incoherent twin boundaries in low stacking fault energy metals form as a narrow slab of 9R stacked material. 9R is equivalent to a close-packed stacking of FCC {111} planes with an intrinsic stacking fault inserted every three planes (i.e., a stacking sequence of ABC/BCA/CBA ...). The factors controlling the formation and stability of such structures are poorly understood. We are collaborating with LLNL (G. Campbell) and the Univ. of Minnesota (C. Barry Carter) to better understand the influence of dislocation structure and strain on grain boundary dissociation.

Accomplishment:

Figure 1 shows an HRTEM image of a copper Σ=3 incoherent twin boundary, fabrication by diffusion bonding at LLNL. The central ~30Å wide region is in the dissociated 9R configuration. Growth of the copper 9R layer, accompanied by a relative shear of the two halves of the bicrystal, was observed *in situ* by HRTEM at Sandia. We have shown that the interfaces terminating the two sides of the 9R layer are well described in terms of two separate arrays of Shockley dislocations: one, an array of pure edge, 90° dislocations (**A**δ) and the other, an array of paired 30° dislocations (**B**δ + **C**δ). Stacking errors in the 9R layer (e.g., the 4- and 5-layer faults indicated on the figure) arise due to the presence of secondary grain boundary dislocations, of Burgers vector $a/6 < \bar{2}11 >$, which accommodate both tilt and twist misorientations from the ideal Σ=3 coincidence. The specific fault type can be explained by considering both the sense (positive or negative) and character (pure edge (90°) or mixed (30°)) of the secondary grain boundary dislocation's Burgers vector. For instance, as shown in Figure 2, addition of a single positive 30° dislocation (**B**δ) to the interfacial dislocation sequence increases the spacing between the pure edge **A**δ dislocations by one plane producing a four-plane fault upon boundary decomposition. Due to glide of the dislocations comprising the interface, the width of 9R dissociation is sensitive to local stress fields. Figure 3 shows results of an atomistic calculation, performed using the Embedded Atom Method, simulating the effect of an applied shear strain parallel to the boundary. In this calculation, the width of the 9R layer has increased through the glide of edge dislocations associated with the kite-shaped figures at the right-most 9R-FCC interface.

Significance:

Our work shows that the dynamics of the 9R growth and the specific defect structures in the 9R layer can be directly related to the dislocation structures of the interfaces terminating the region of dissociation. These results provide insight into the issues controlling grain boundary dissociation, which appears to be an important mode of interfacial relaxation in low stacking fault energy metals.

Reference:

"Stacking Defects in the 9R Phase at an Incoherent Twin Boundary in Copper,"
D.L. Medlin, G.H. Campbell, and C. Barry Carter, submitted to *Acta Materialia*.

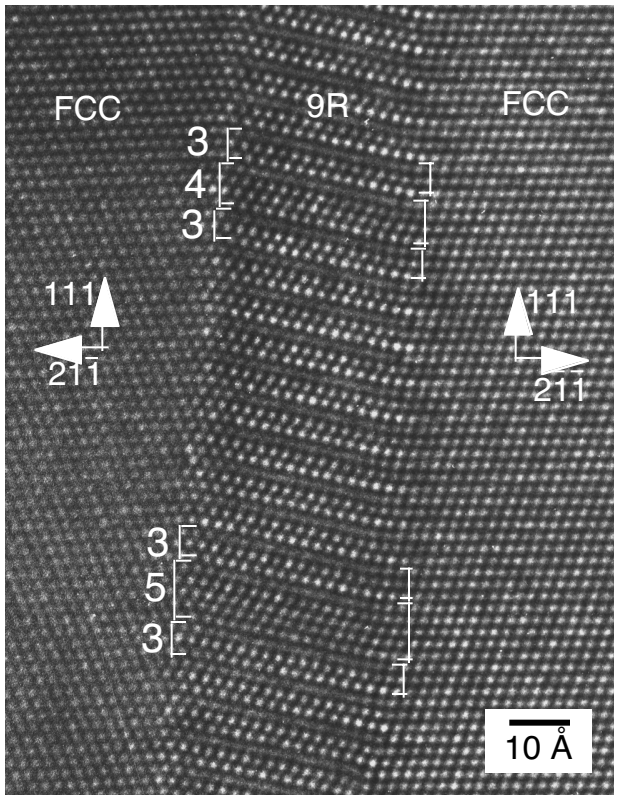

Figure 1. HRTEM image showing 9R region at dissociated Cu incoherent twin boundary. 4- and 5-layer faults in the 9R stacking are indicated.

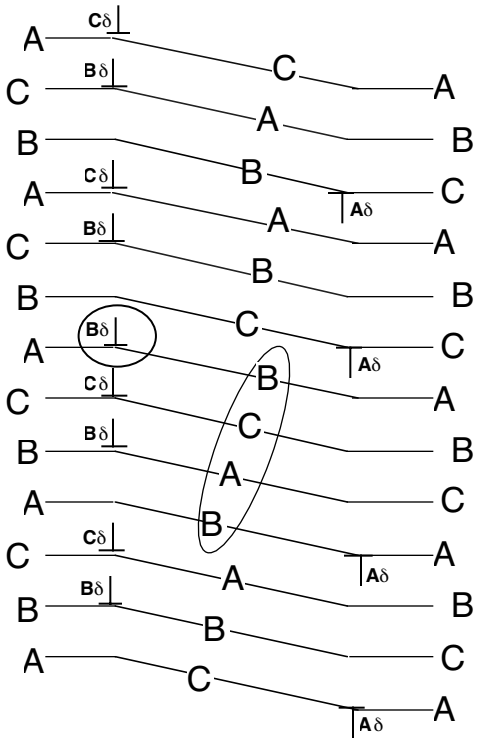

Figure 2. Schematic showing the formation of a 4-layer fault in the 9R layer by insertion of a positive 30° dislocation (**B**δ).

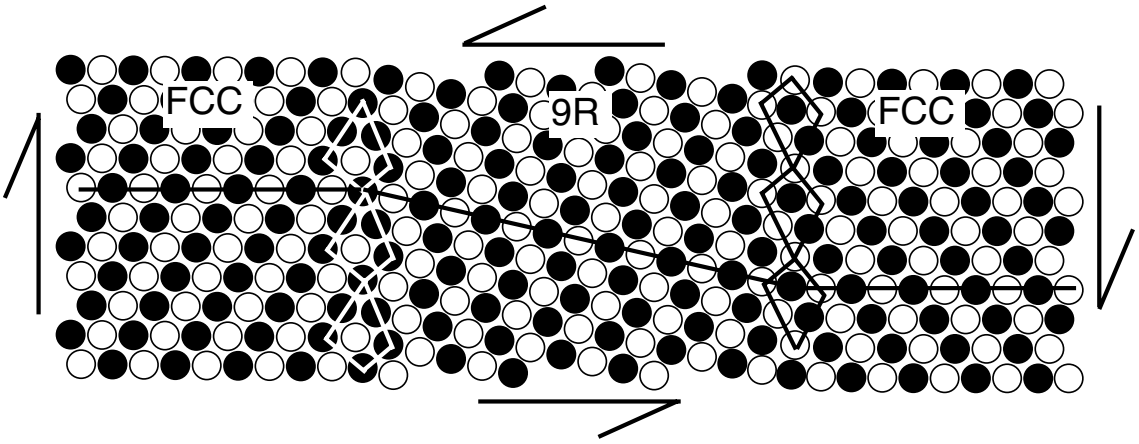

Figure 1. Atomistic simulation showing wide 9R region resulting from application of shear parallel to interface.

Observations and Modeling of Grain Boundary Dislocation Structure

D.L. Medlin and S.M. Foiles

Motivation:

The interaction of lattice dislocations with grain boundaries and the motion of grain boundary dislocations and ledges on grain boundaries play important roles in controlling the dynamics of grain boundary processes in polycrystalline materials. Dissociation of a lattice dislocation at a grain boundary can produce additional interfacial dislocations, which may then contribute to further deformation by moving along the interface. Understanding the structure and properties of such defects can thereby aid in understanding the overall behavior of grain boundaries.

Accomplishment:

Using high resolution transmission electron microscopy (HRTEM) and atomistic simulations, we have studied the structure of a/3[111] grain boundary dislocations on a $\Sigma=3\{\bar{2}11\}$ incoherent twin boundary in aluminum. Because the Burgers vector of these dislocations lies in the plane of the boundary they are able to move by glide, providing a mechanism for grain boundary sliding. Such defects can originate at this interface via a lattice dislocation decomposition reaction of the type: $a/2[011] \rightarrow a/3[111] + a/6[\bar{2}11]$. The resulting a/3[111] dislocation can dissociate further into two partial grain boundary dislocations that separate structurally equivalent regions of opposite rigid body translation. Figure 1 shows an experimental HRTEM image and an atomistic simulation of one such partial grain boundary dislocation (**b**=a/9[111]). The translation state changes continuously along the length of the interface: at the top of the figure the horizontal (111) planes bend downward across the interface, whereas at the bottom, the planes bend upward. From both experimental measurements and atomistic simulations we have learned that these dislocations have wide core configurations. To quantify this width we have analyzed the calculated atom positions in terms of a functional form based on a Peierls-Nabarro type dislocation model. From this fit, the dislocation core widths for the a/9[111] and 2a/9[111] dislocations in the atomistic model are characterized as 49 Å and 23 Å, respectively.

Significance:

Such large cores result in a significant interaction even for widely spaced dislocations. Figure 2, plots the calculated displacement function for an array of dissociated a/3[111] dislocations spaced at 350Å intervals. Although the curvature changes at the positions of the partial grain boundary dislocations, at no point does the structure relax to form regions of constant displacement. Thus, unlike the undislocated, perfect interface, which has a constant rigid body displacement across the interface of approximately $1/3d_{111}$, the interface with an array of dislocations exhibits a continuous variation in structure. This result demonstrates the dramatic effect of long range dislocation strain fields on grain boundary structure.

Publications:

"Climb and Glide of a/3<111> Dislocations in an Aluminum Σ=3 Boundary"
D.L. Medlin, et al., *Philosophical Magazine* A 75 (3) (1997) 733-747.

"Grain Boundary Dislocation Structure and Motion in an Aluminum Σ=3 [011] Bicrystal" D.L. Medlin, S.M. Foiles, C.B. Carter, in *Atomic Resolution Microscopy of Surfaces and Interfaces*, MRS Proc. 466, eds. D.J. Smith and R.J. Hamers, (1997) 125-130.

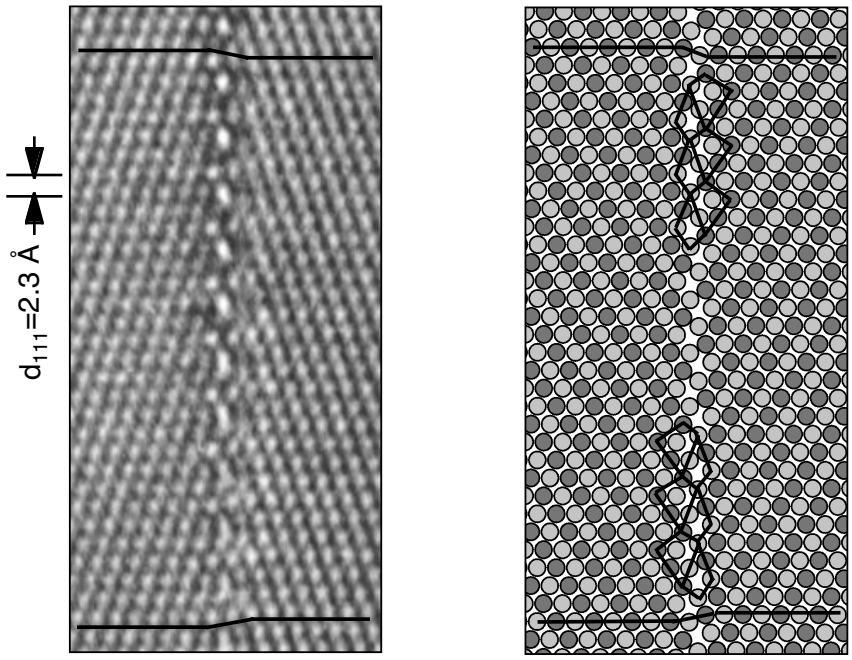

Figure 1. (a) Experimental HRTEM image showing reversal in (111) fringe displacement at an a/9[111] partial grain boundary dislocation on a Σ=3 {11$\bar{2}$} interface in aluminum. (b) Defect structure calculated using the EAM.

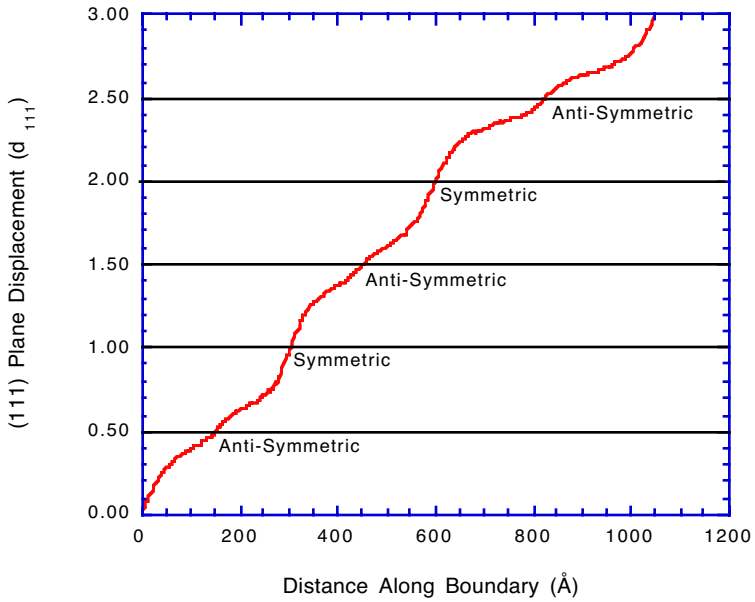

Figure 2. Calculated (111) plane displacement along interface for an array of a/3[111] dislocations initially spaced at 350Å intervals. Changes in curvature correspond to the positions of the two types of partial grain boundary dislocations: a/9[111] (anti-symmetric, 2a/9[111] (symmetric).

Atomistic Models of Dislocation Nucleation during Nanoindentation

C.L. Kelchner and J.C. Hamilton

Motivation:

The continuing drive to reduce the size of electrical and mechanical devices is forcing materials science into domains where conventional ideas must be subject to careful scrutiny. As length scales decrease, atomistic effects play an ever increasing role and continuum analysis will eventually no longer be adequate. One of the classic tests for materials properties is indentation, used to determine hardness, elastic moduli, and adhesive properties of films. Smaller and smaller "indenters" have been developed including the nanoindenter, the atomic force microscope, and the interfacial force microscope. These instruments provide novel new measurements of mechanical properties on extremely small length scales relevant to new applications. Recent observations have shown that ideas regarding plastic thresholds which were developed for macroscopic indenters are not reliable at the spatial scale of some of the new instruments. The present theoretical work was motivated by the necessity to understand dislocation nucleation under indentation at these spatial scales. Exactly where and how the initial dislocations form has been largely a matter of speculation. The properties of a material are known to be affected by the dislocation structure, and understanding the nucleation process may lead to better control over these introduced defects. We have performed atomistic calculations of the nucleation of dislocations during indentation to resolve this issue. This theoretical work is directly coupled to experimental work in a related Sandia N.M. BES program on interfacial adhesion.

Accomplishment:

We have modeled indentation by combining a frictionless indenter with atomistic calculations. In order to study the defect structure of the indented surface in detail, the location and type of defects present must be reliably identified and separated from the extensive elastic deformation in the system. We have developed a general solution to this problem for a centrosymmetric material which relies on the fact that homogeneous elastic deformation does not break centrosymmetry. This solves a long standing problem in the imaging and interpretation of atomistic calculations of dislocation structures. The system chosen for study was a Au(111) surface which was passivated to prevent adhesion between the indenter tip and the surface. Our calculations show that the dislocations nucleate on the {111} glide planes just below the surface then grow into the bulk lattice. A snapshot of the system near the beginning of this nucleation process is presented in Figure 1, with stacking faults shown as dark gray and partial dislocations as light gray (surface atoms are also shown in white). The structure formed after these initial dislocations finish growing is shown in Figure 2.

Significance:

This work provides the first atomistic imaging of dislocation nucleation during indentation of a passivated surface. Although the maximum shear stress from continuum theory is centered underneath the indenter at a depth of about half the contact radius, our results clearly show that this is not where the dislocations nucleate. This implies that the commonly used criterion for plastic yield in a material, i.e., that the maximum shear stress under the indenter exceed the theoretical shear stress of the material, is at best a crude approximation. In addition, these atomistic calculations provide the complex asymmetric defect structure that results from the initial dislocations and which had been previously unavailable. We believe that the dislocation imaging technique developed here is superior to any existing technique and will find wide applicability in theoretical modeling of defect structures in centrosymmetric materials.

Publications:

"Dislocation structure during surface indentation of passivated Au(111)," C. L. Kelchner, S. J. Plimpton, and J. C. Hamilton, submitted to Physical Review Letters.

Figure 1. Snapshot of the initial stage of dislocation nucleation during indentation of Au(111). The shading indicates defect types: partial dislocation (dark gray), stacking fault (light gray), and surface atoms (white). The atoms in regions having only elastic strain are not shown. The surface deformation is due to the indenter pressing into the surface.

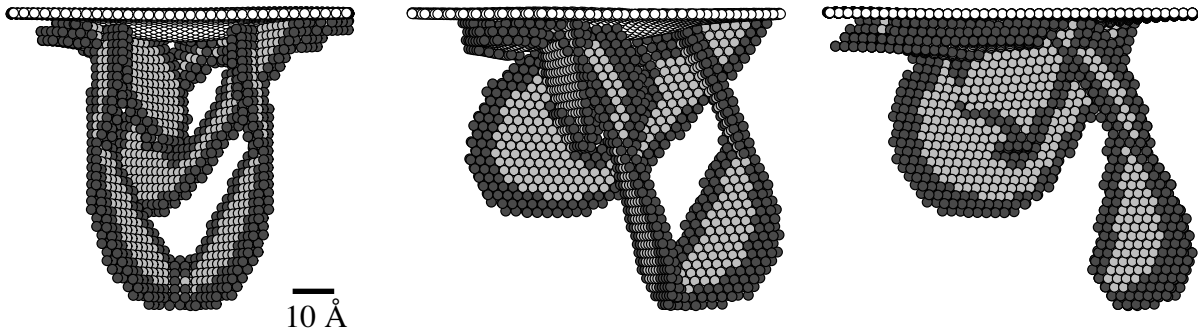

Figure 2. Equilibrium defect structure at the onset of plastic deformation during indentation of Au(111), (a) view along $[11\bar{2}]$, (b) rotated 45˚ about [111], and (c) rotated 90˚ to $[1\bar{1}0]$. The shading indicates defect types as in Figure 1. The viewing direction is identical in Figure 2(a) and in Figure 1.

New Scaling Relationships for Dislocation Microstructures in Deformed Metals

D. A. Hughes and A. Godfrey, Sandia National Laboratories, Livermore, California; D. C. Chrzan, UCB; Q. Liu and N. Hansen, Risø Nat. Lab., Roskilde, Denmark

Motivation -- Large strain deformation takes place in many metal forming processes such as sheet forming, forging, extrusion, and sheet rolling. In all these cases, the plastic deformation creates a subdivision of the initial grains into smaller crystallites separated by dislocation boundaries and high angle boundaries, and gives rise to a preferred texture. While the dislocation cell formation and grain refinement have been described qualitatively, a further step is to quantify structural parameters that integrate the microstructure into constitutive laws. The discovery of the scaling relationships described below indicate that general relationships do exist which control the evolution of the dislocation structure as a function of the plastic deformation.

Accomplishment -- A range of metals and alloys have been deformed in different ways to different strain levels, including compressed pure aluminum single crystals, cold rolled aluminum polycrystals, cold rolled nickel polycrystals and high temperature compressed 304L stainless steel. Transmission electron microscopy and convergent beam Kikuchi analysis were performed on the deformed samples to measure the dislocation boundary spacing and misorientation angles. Two different types of dislocation boundaries were identified. Long, continuous dislocation boundaries that have been called geometrically necessary boundaries (GNBs), and smaller scale cell boundaries termed incidental dislocation boundaries (IDBs). For a given material, the average misorientation angle increases while the boundary spacing decreases with increasing stress and strain for both types of boundaries. The probability densities of misorientation angles, $P(\theta, \theta_{av})$ (Fig. 1a), and boundary spacings $P(D, D_{av})$ were calculated for each boundary type from the experimental data. Although each distribution is very different, it was discovered that they can all be scaled according to: $P(\theta,\theta_{av}) = \theta_{av} f\left(\theta / \theta_{av} \right)$.

For the boundary spacings equation, D and D_{av} replace θ and θ_{av}. For the range over which both parameters scale, $D_{av}\theta_{av}$ is a constant for a given material. While the scaling applies to all distributions for the IDBs, Fig. 1b, small deviations are found for the GNBs, as can be seen from Fig. 2. The deviations may be caused by additional factors controlling the GNB misorientation distribution especially at larger strains. The scaling of misorientation angles breaks down above a strain $\varepsilon=1$, whereas the scaling relation for boundary spacings (Fig. 3) holds to very large strains $\varepsilon=4.5$.

Significance -- The distributions of misorientation angles for different materials, different deformation modes and different plastic strains are all characterized by a single function with one characteristic parameter, the average misorientation angle. This average value evolves with increasing strain and reflects the microstructural differences due to the material and deformation mode. Importantly, the same scaling relationships can be made for the boundary spacings which are related to the flow stress. The existence of the scaling relationship for the misorientations and spacings indicates that the deformation structure and its evolution are governed by relatively simple laws for the collective properties of dislocation microstructures produced by plastic deformation. Therefore the scaling relationships will be very useful to analyze and model microstructure evolution and to quantitatively describe microstructural parameters that control the strength.

Publications -- D. A. Hughes, Q. Liu, D. C. Chrzan, and N. Hansen, "Scaling of Microstructural Parameters: Misorientations of Deformation Induced Boundaries," *Acta Mater.,* 45, (1997), 105-112; A. Godfrey and D. A. Hughes, "Scaling of Dislocation Wall Spacings," in preparation.

a) b)

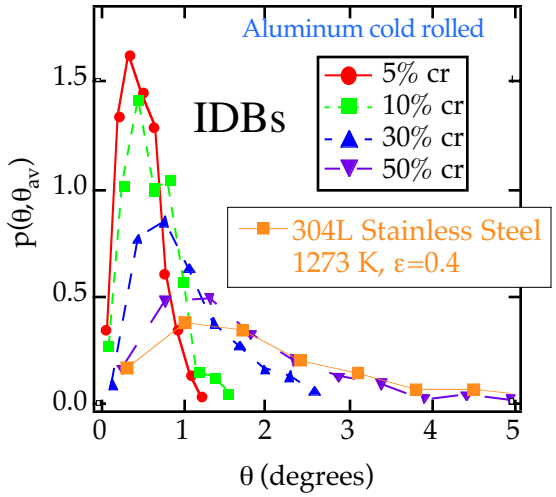

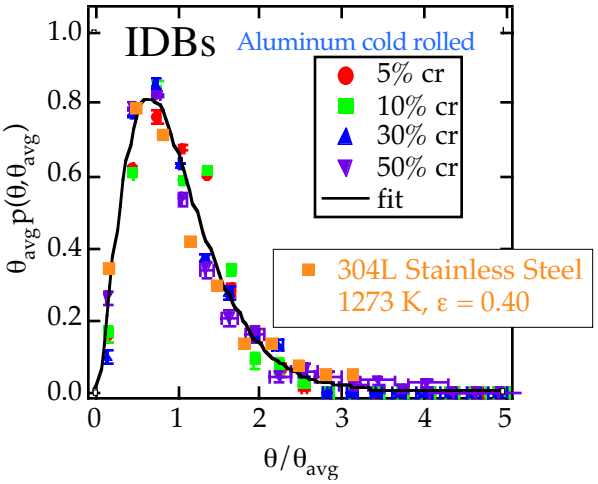

Fig. 1 a) Probability densities of the IDB boundary misorientation angles. b) Misorientation angle probability densities scale into one distribution

a)

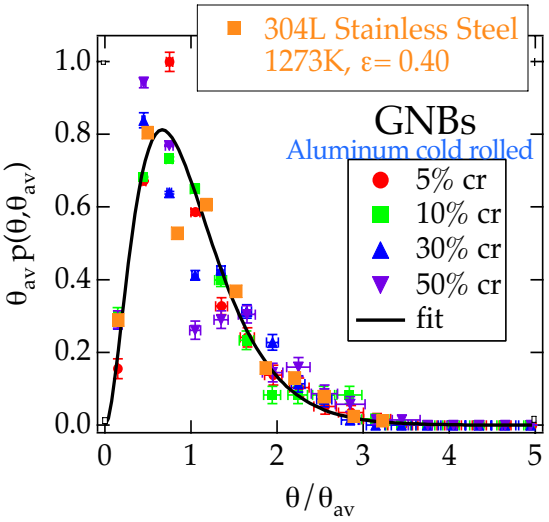

Fig. 2 Misorientation angle probability densities of GNBs scale into one distribution.

b)

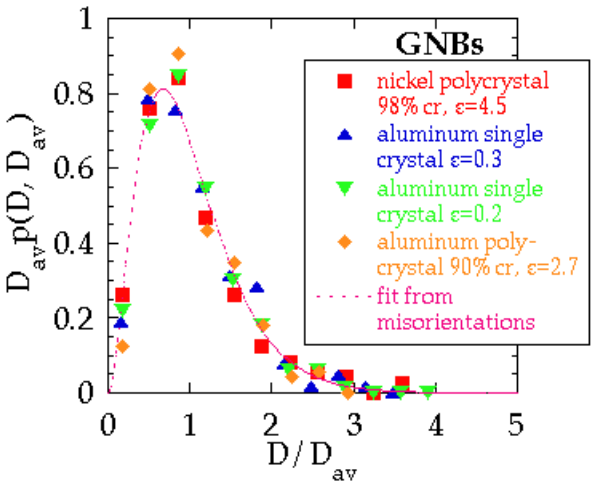

Fig. 3 Probability densities of boundary spacings for GNBs scale into one distribution that is similar to that for the misorientation angle.

Ordered vacancy island lattices in a strained metal film

K. Pohl, N.C. Bartelt, J. de la Figuera, M.C. Bartelt and R.Q. Hwang

Motivation:

Elastic interactions between defects on surfaces have been conjectured to account for many observations of "self assembly" on surfaces. For example, the regularity of arrangements of islands often observed during heteroepitaxial growth is usually attributed to elastic interactions between the step edges of the islands. These elastic forces, however, have never been directly measured. Measuring energies on surfaces using microscopy is, of course, an extremely difficult problem. In our work we have taken the approach of using observations of thermal fluctuations of an ordered array of surface defects to probe the interactions between the defects.

Accomplishment:

Figure 1 shows an STM image of an ordered vacancy island lattice formed on exposing a monolayer of Ag on Ru(0001) to sulfur. This is a particularly well-defined example of a "mesoscopic" surface structure: each vacancy island is about 1.2nm in radius; the spacing between islands is about 5.2nm. Isolated vacancies islands are observed to move extremely rapidly at room temperature — tens of nanometers per minute. Thus there is clearly a strong repulsive interaction between the islands keeping them from coalescing when their density is high. To probe this interaction we have characterized the thermal vibrations of each island about its equilibrium lattice position (Fig. 1(b)). Just as phonons in normal solids can be used to probe interactions between atoms in a solid, the thermal vibrations of the vacancy hole array can be used to probe the "mesoscopic" ordering forces.

Figure 2 shows a histogram of the position of the center-of-mass of an island. The gaussian form of the histograms shows that each island appears to vibrate in a harmonic well. This harmonicity suggests that the vibrations can be characterized by a normal mode (phonon) analysis of the vibrations. Performing such an analysis allows us to estimate the bulk modulus of the vacancy lattice to be on the order of 2×10^{6} Pa. This order-of- magnitude is consistent with theories of interactions between steps in strained films.

Significance:

By comparing the measured elastic constants of the vacancy island lattice with models of interactions between steps we have been able to probe the fundamental properties of the Ag film which are responsible for mesoscopic ordering observed in thin metal films.

Publications:

Ordered vacancy island lattices in a strained metal film, K. Pohl, J. De la Figuera, M.C.Bartelt, N.C. Bartelt , R.Q. Hwang and J. Hrbek, in preparation.

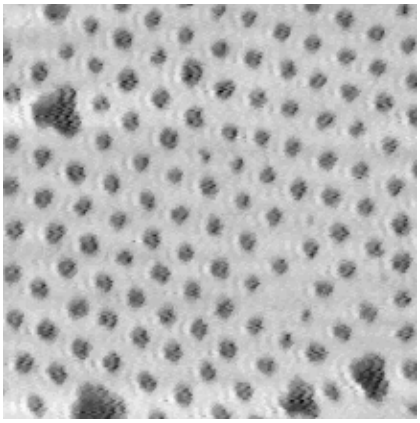

Figure 1(a) 60nm×60nm STM image of vacancy islands in a (strained) monolayer of Ag on Ru(0001).

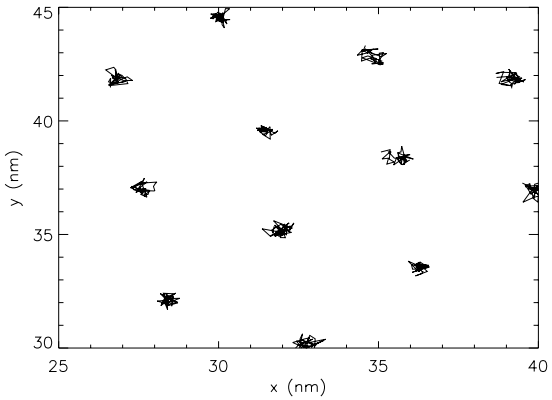

Figure 1(b) Trajectories of the centers of mass of some of the vacancy islands in Fig. 1(a).

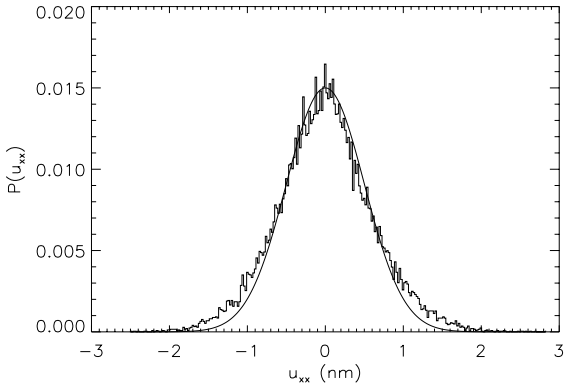

Figure 2 Histogram of displacements of the position of the center of mass of a vacancy island.

HRTEM Study and First-Principles Modeling of the Al(111)-Al_2O_3(0001) Interface

P. Tepesch, M.D. Asta and A.A. Quong

Motivation:

Metal-ceramic bonding is an important materials issue in many technological applications, including micro-electronics where the properties of metal-ceramic interfaces and the details of interface formation are critical. The Al-Al_2O_3 system is important technologically (for example in hybrid circuits), and is also a simple model system for studying metal-ceramic interfaces.

Accomplishments:

Atomically sharp Al- Al_2O_3 interfaces were formed by deposition of Al onto single-crystal Al_2O_3 (0001) substrates. The Al was found to be oriented with the (111) direction perpendicular to the substrate surface with two predominant orientations parallel to the interface related by a 180 degree rotation. As shown in figure 1, the HRTEM images of this interface do not resolve the details of the atomic structure at the interface. To understand these details, we have applied first-principles electronic structure calculations to model the relaxed structure and energy of six models for the coherent Al(111)- Al_2O_3(0001) interface shown in figure 2. The models were constructed from the three possible surface terminations of Al_2O_3 (0001) derived by terminating the bulk stacking sequence in contact with a perfect Al(111) surface in the two rotations observed experimentally (the Al was compressed to the Al_2O_3 in-plane lattice parameter.) The energy of the models (given in the table below) were minimized with respect to the separation of the layers and the atomic positions.

	Interfacial Energy (J/m^2)		
Orientation	"O-terminated"	"1Al-terminated"	"2Al-terminated"
0 degrees	2.58	2.58	2.16
180 degrees	2.63	2.64	1.85

For comparison, the intrinsic stacking fault energy in Al is approximately 0.1 J/m^2. Since the "2Al-terminated" interface model had the lowest interfacial energy and the two orientations had a very high difference in interfacial energy, we considered one more model that consists of a stacking fault in the Al layer, two (111) planes away from the interface. This also results in a 180 degree rotation. For the lowest energy interface ("2Al-terminated", 0 degrees), the interfacial energy changed only by 0.001 J/m^2. This suggests that the two orientations of the Al might be observed as a result of a reduced stacking-fault energy near the metal-ceramic interface.

Significance:

The HRTEM images in conjunction with the first-principles calculations have clarified the nature of the atomic structure of the Al(111)-Al_2O_3(0001) interfaces. The first-principles calculations suggest that the reduction in the stacking fault energy near the interface may be the reason two orientations of Al are observed. This idea may help explain similar behavior in other metal-Al_2O_3 interfaces.

Publication:

P. Tepesch, M.D. Asta and A.A. Quong, in preparation.
D.L. Medlin, K.F. McCarty, R.Q. Hwang, S. Guthrie, and M. Baskes "Orientation Relationships in Heteroepitaxial Aluminum Films on Sapphire," Thin Solid Films 299 (1997) 110-114.

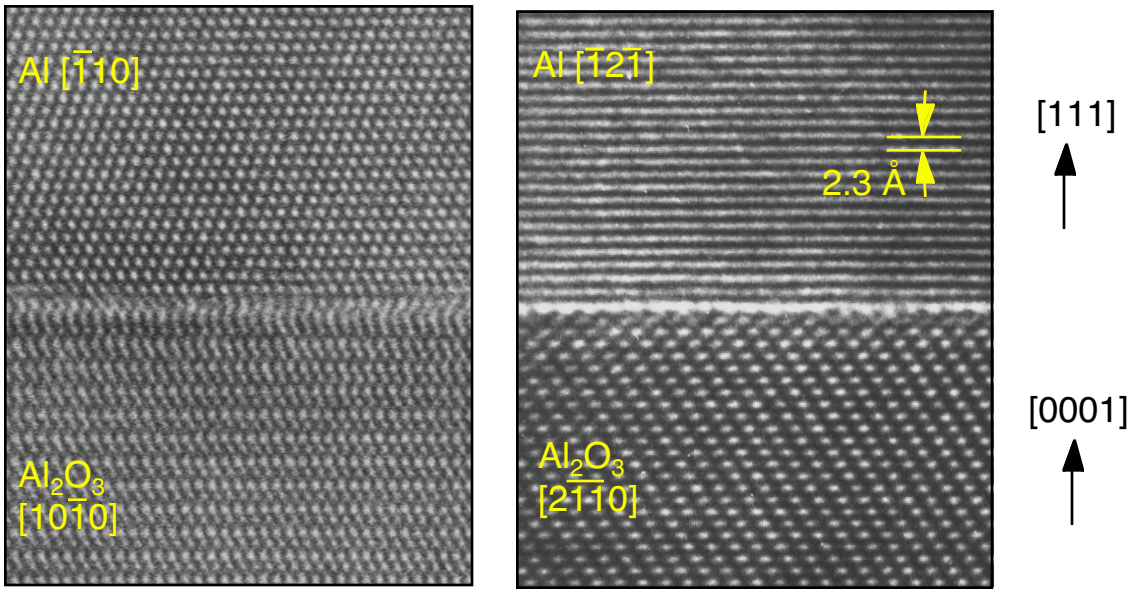

Figure 1: HRTEM images of the atomic-scale structure of the Al(111)-Al2O3(0001) interface.

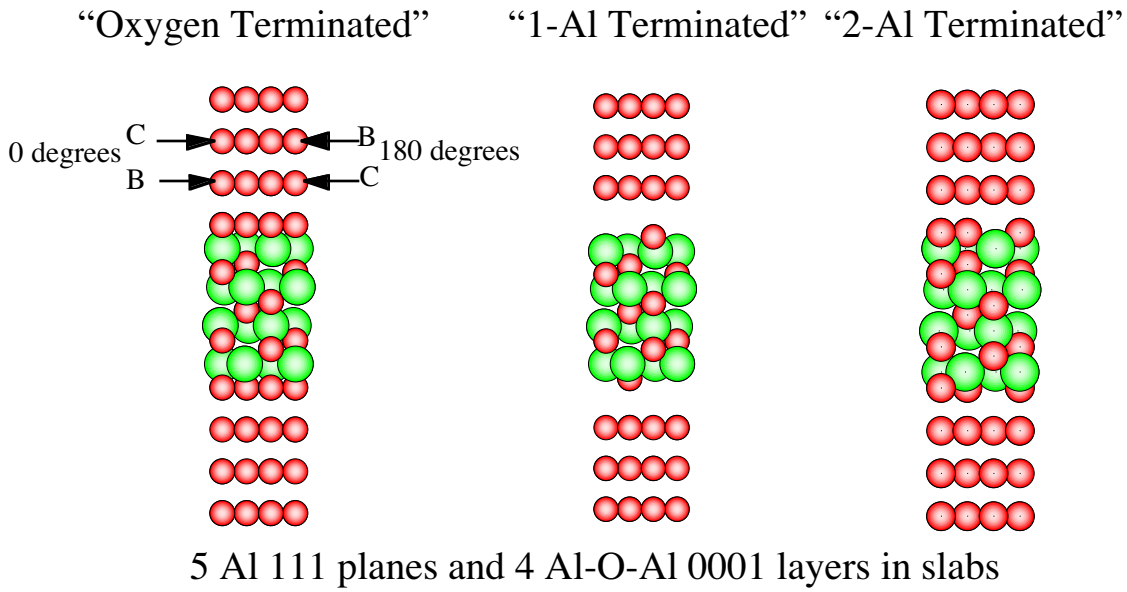

Figure 2: Models for the coherent Al(111)-Al_2O_3(0001) interface.

Predicting Complex Grain Structure Dynamics of Prototypical Thin Films

A.K. Schmid, N.C. Bartelt and R.Q. Hwang

Motivation:

Grain structure in polycrystalline thin films can profoundly affect mechanical, electrical, and chemical properties. Thermally activated motion of grain boundaries is the key phenomenon by which thin film grain structure evolves. A detailed theoretical understanding of grain boundary motion therefore has great technological importance. Ultimately, one would like to be able to predict thin film grain structure from a knowledge of the properties of the film atoms. Using a prototypical polycrystalline thin film, we show how on a mesoscopic scale involving large numbers of atoms, the detailed time evolution of complex grain structures can be successfully predicted from an analysis of the random thermal motion of the film atoms.

Accomplishment:

As a simple polycrystalline thin film system, we have studied oxygen adsorbed on Ru(0001). Near a coverage of a quarter of a monolayer, oxygen forms a p(2x2) structure. This structure has four degenerate ground states, corresponding to the four different Ru(0001) sublattices of binding sites that the p(2x2) unit cell can occupy. As a consequence of this degeneracy, Ru(0001) surfaces which are rapidly exposed to O_2 contain complicated networks of randomly nucleated p(2x2) grains. The grain boundaries separating these domains raise the free energy of the system and are gradually removed by a coarsening process in which large domains grow at the expense of smaller ones. Using scanning tunneling microscopy (STM), we are able to quantify this relaxation process on an atomic scale, and relate what the atoms are doing to the overall surface configuration. Two atomically resolved images of the same grain boundary in a p(2x2) oxygen adlayer, shown in Fig. 1, illustrate the random motion of atoms crossing the grain boundary on a scale of a few seconds. On larger time and length scales, this random atomic motion allows the system to lower its free energy by reducing grain boundary length. In Fig. 2(a) and (b) larger STM images taken four hours apart show this gradual coarsening.

In this system, we can successfully validate the basic theory of grain boundary mobility. To construct a computationally convenient model, we have used the analogy with the four-state Potts model to perform Monte Carlo simulations. Excellent agreement of the simulation result in Fig. 2(d) with the experimental data in (b) highlights the accuracy with which the computational model can predict the grain coarsening of the real physical system on a scale involving some 10^5 atoms.

Significance:

The challenge in describing grain coarsening is to account for the large scale motion of grain boundaries on the basis of atomic scale information. While the O/Ru(0001) system is too idealized to show all of the characteristics of grain coarsening generally, it does allow the usefulness of standard models of grain growth to be demonstrated in atomic detail in a real physical situation. This work shows how one can reasonably expect to predict how actual (and thus usually complex) grain configurations evolve with time, starting with equations of motion derived from atomic observations.

Publications:

"Predicting the Future of a Complicated Surface Structure: Grain Coarsening of p(2x2)O/Ru(0001)", in press Phys. Rev. Lett., A.K. Schmid, R.Q. Hwang, and N.C. Bartelt

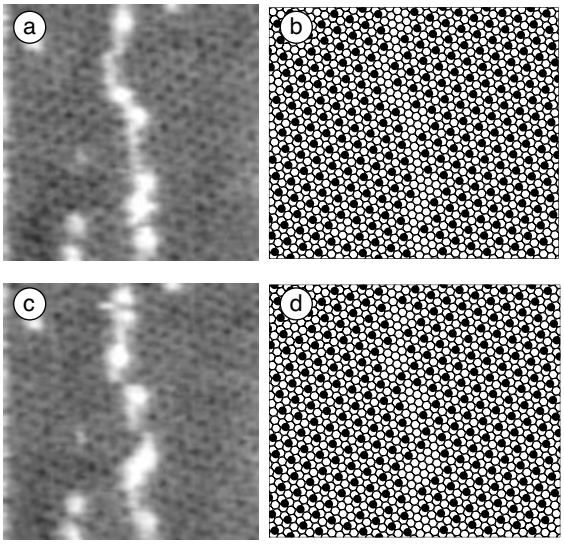

Fig. 1: (a) A 9 nm x 9 nm STM image of an antiphase domain boundary in p(2x2) O/Ru(0001). The dark spots are O adatoms, bright spots are advacancies. (b) Chart of the adatom positions shown in (a). Panels (c) and (d) show the adatom configuration 7 s later.

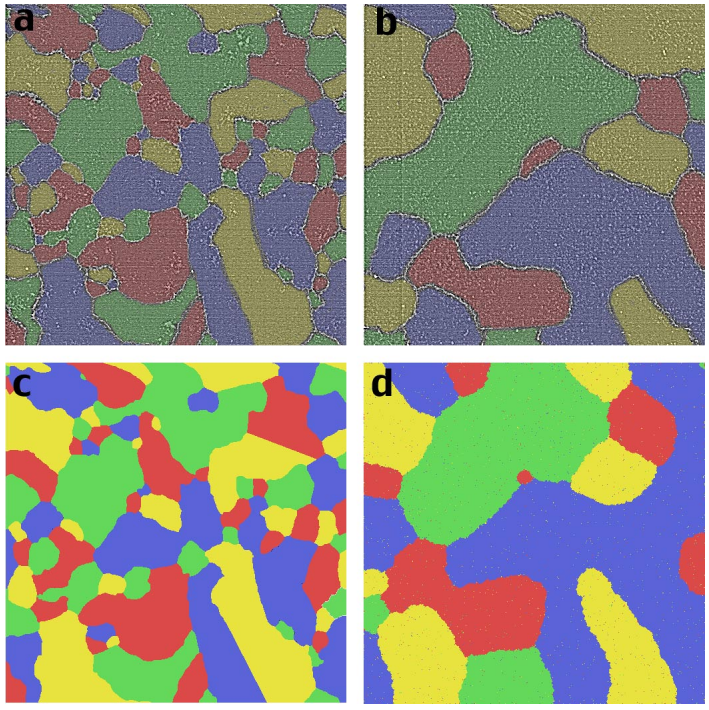

Fig. 2: Late stage coarsening in the system p(2x2) O/Ru(0001). (a) 350 nm x 350 nm STM image of the oxygen (2x2) film. (b) Same area imaged again nearly 4 hours later. Antiphase domain walls in the adlayer appear as white lines in the STM images. Grayscale was manually superimposed into the data to highlight domains. The configuration of domains shown in (a) was digitized to provide an initial configuration for the Monte Carlo simulation, (c). Propagating this configuration forward in time produced the configuration (d) after 7500 Monte Carlo steps-per-site.

ISLAND SIZE DEPENDENCE OF ADATOM CAPTURE:
Cu/Co ISLANDS ON Ru(0001)

M.C. Bartelt, A.K. Schmid and R.Q. Hwang

Motivation:

A general feature of metal-on-metal epitaxy is that the configuration of the growing film typically cannot relax to equilibrium on the time scale of deposition. Thus a variety of far-from-equilibrium morphologies can be produced (cf. Fig.1), many of which have increasing technological value. In the submonolayer regime, a distribution of islands is typically formed, at low substrate temperatures, following random deposition of atoms on to, and diffusion of adatoms between, adsorption sites defined by the substrate. Competition between different islands for the capture of diffusing adatoms controls the details of the resulting island distribution. Specifically, we have shown recently using a simple model that the dependence of the rate of capture of diffusing adatoms on the island size determines the shape of the island size distribution. The exact form of that dependence, as determined in our simulations, was found to differ qualitatively from widely accepted mean-field predictions. However, direct comparison of results from simulations for realistic island geometries, and from mean-field analysis, with experiment was missing.

Accomplishment:

With sophisticated STM experiments, we were able to quantify the rate of capture by Co islands on Ru(0001) of additionally deposited Cu atoms, determining its key dependence on Co-island size. This is the first experimental analysis of this quantity and of its "island environment dependence".[1] As found in simulations,[2,3] the dependence on island size reflects larger island-free areas surrounding bigger islands, i.e., a strong correlation between island sizes and separations. See Fig.2. This feature is neglected in mean-field treatments, where the environment of each island is assumed independent of island size (and shape). Furthermore, we exploited the limited rearrangement of Cu adatoms around the perimeter of the Co islands, to assess, in addition to the magnitude, the direction dependence of adatom capture. For a distribution of islands matching experiment, we quantified these features (i) via stochastic simulations of deposition, diffusion, and eventual capture of adatoms by islands; and (ii) by solving an appropriate diffusion equation.

Significance:

Submonolayer structures can influence the morphology and properties of multilayer thin films. Precise description of island formation is thus a pre-requisite for systematic control of non-equilibrium film structure and properties. Other fundamental processes, including cluster coagulation or chemical reactions in a fluid, are mediated by diffusion. Like for island nucleation and growth during film deposition, general analysis depends on the specification of the cluster size dependence of the aggregation rates, for which only mean-field-like theories are typically available. Our study is the first combined and consistent analysis of results from experiment and theory for the island size dependence of adatom capture[1], following the first detailed characterization of its non-mean field behavior[2,3].

Publications:

[1] Island size dependence of adatom capture: Cu/Co islands on Ru(0001), M.C. Bartelt, A.K. Schmid, J.W. Evans, and R.Q. Hwang, submitted to Phys. Rev. Lett..

[2] Exact island-size distributions for submonolayer deposition: Influence of correlations between island size and separation, M.C. Bartelt and J.W. Evans, Phys. Rev. B **54** (1996) R17359.

[3] Submonolayer nucleation and growth of 2D islands and multilayer mound formation during homoepitaxy, M.C. Bartelt and J.W. Evans, to appear in *Morphological Organization in Epitaxial Growth and Removal*, edited by Z. Zhang and M.G. Lagally (World Scientific, Singapore 1998).

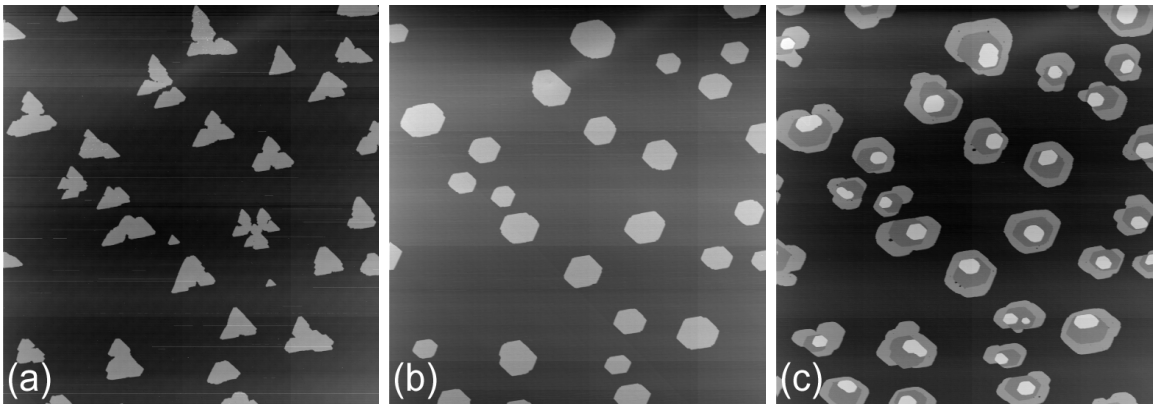

1. (a) Non-equilibrium distribution of Co islands obtained in UHV during deposition of 10% of a monolayer of Co on Ru(0001), at 50°C. The equilibrium island shape is nearly hexagonal, as obtained in (b) after a flash anneal to 350°C. The equilibrium configuration for this adlayer would consist of a single 2D large region of Co coexisting with a dilute 2D "gas" of Co adatoms. (c) The same region as in (b) after deposition of 25% of a monolayer of Cu at room temperature. Co islands are decorated with rings of Cu. Cu atoms deposited directly on top of the islands formed second-layer islands. STM images are 500×500 nm^2, and were taken at room temperature. Brighter regions have higher corrugation.

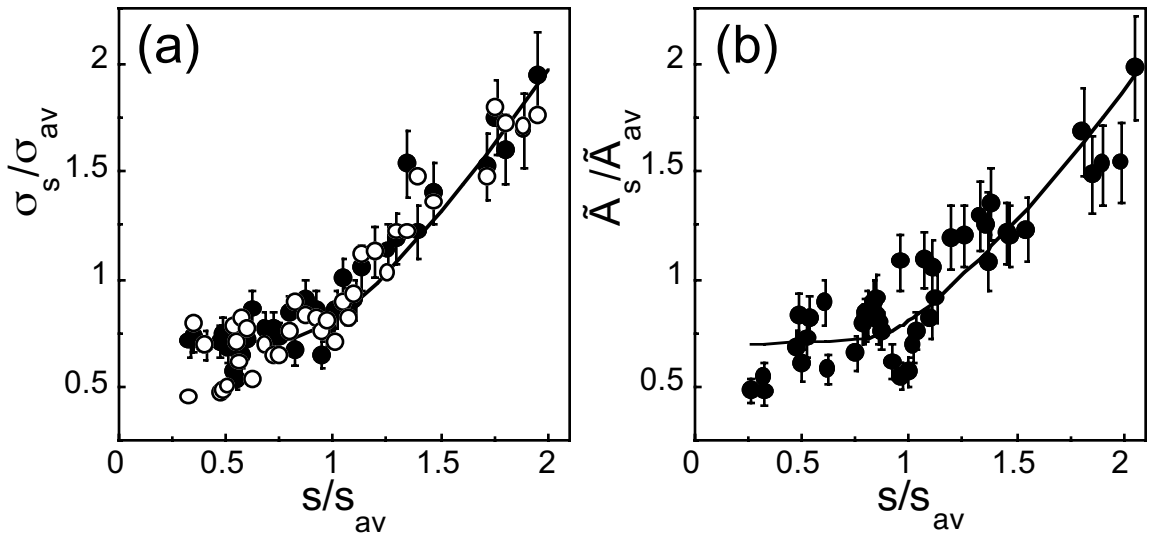

2. Results of the analysis of a 1.2×1.2 μm^2 STM image, with about 100 islands. Solid (open) symbols are experimental (simulation) data. (a) The fraction, σ_s/σ_{av}, of Cu adatoms captured by each island, versus island size (both normalized by the average). (b) The dependence on island size of the relative area, $\tilde{A}_s/\tilde{A}_{av}$, of cells in a Voronoi tesselation of the adlayer. Each Voronoi cell corresponds to the region of the surface closer to the center-of-mass of an island than to those of other islands. The areas of the Voronoi cells are in approximate proportion to the average capture by each island. In fact, one finds $\sigma_s/\sigma_{av} \approx 1.2(\tilde{A}_s/\tilde{A}_{av})-0.2$, which specifically quantifies the connection between adatom capture and the average local environment of an island of size s.

ANISOTROPIC DIFFUSION OF ATOMS AROUND ISLAND EDGES ON METAL (110) SURFACES

M.C. Bartelt

Motivation:

Processes leading to transport of atoms between island edges control island shape equilibration during film growth. When such processes are inefficient on the time scale of capture of diffusing adatoms by growing islands, fractal, dendritic, or strongly anisotropic chain-like islands can be observed. Examples of the latter include Si islands grown on Si(001), or Cu islands grown on Pd(110), at low temperatures. Specifically for this metal system, detailed STM studies have revealed a dramatic transition from chain-like to two-dimensional island growth shapes with substrate temperature increasing above 265K. See Fig.1. A basic question then is whether anisotropy in terrace diffusion (with easy diffusion parallel to the long edge of the Cu islands, along the troughs of the (110) surface) can drive this transition, as had been speculated, or if, instead, it is the anisotropy in bonding of adatoms at island edges that leads to the anisotropy in the transport of atoms between island edges. If it was the former, then 265K would correspond to the temperature at which terrace diffusion becomes isotropic. The latter was previously proposed for Si/Si(001), where easy diffusion is perpendicular to the long edge of the islands. However, rigorous scrutiny of these different scenarios, detailed analysis of measured island aspect ratios, and determination of key parameters for controlling the transition had never been attempted.

Accomplishment:

We developed and tested a model for submonolayer epitaxial growth on anisotropic metal (110) surfaces that can quantitatively reproduce the observed temperature dependence of the island growth shape during submonolayer deposition of Cu on Pd(110). See Fig.2. Simulations, together with experiment, reveal that while there is anisotropy in surface diffusion in this system, as expected for metal (110) surfaces, it is the anisotropy in diffusion around corners at island edges, i.e., the direction-dependent efficiency of transport between island edges, that controls the transition in island shapes with increasing temperature. In fact, anisotropy in terrace diffusion is not needed to produce the island shape transition. The anisotropy in corner rounding, the rounding from [001] to [1$\underline{1}$0] island edges being more difficult than in the reverse direction, derives from anisotropic bonding at island edges, presumably as for Si/Si(001) although the specific kinetic pathway for mass transport between island edges is likely different in the two systems.

Significance:

We have demonstrated the general importance of anisotropy in corner rounding for island growth shape transitions in epitaxy on anisotropic surfaces. Corner and kink rounding are also of general importance in determining non-equilibrium island shapes during epitaxy on isotropic metal (111) surfaces. Indeed, the detailed features of these processes control the initial arm thickening and shape evolution of fractal or dendritic islands, often observed at low temperatures in these systems, and are crucial in quenching such shape instabilities at higher temperatures.

Publications:

Transition from one- to two-dimensional island growth on metal (110) surfaces induced by anisotropic corner rounding, Y.Li, M.C.Bartelt, J.W. Evans, N. Waelchli, E. Kampshoff, and K. Kern, Phys. Rev. B **56** (1997) 12539.

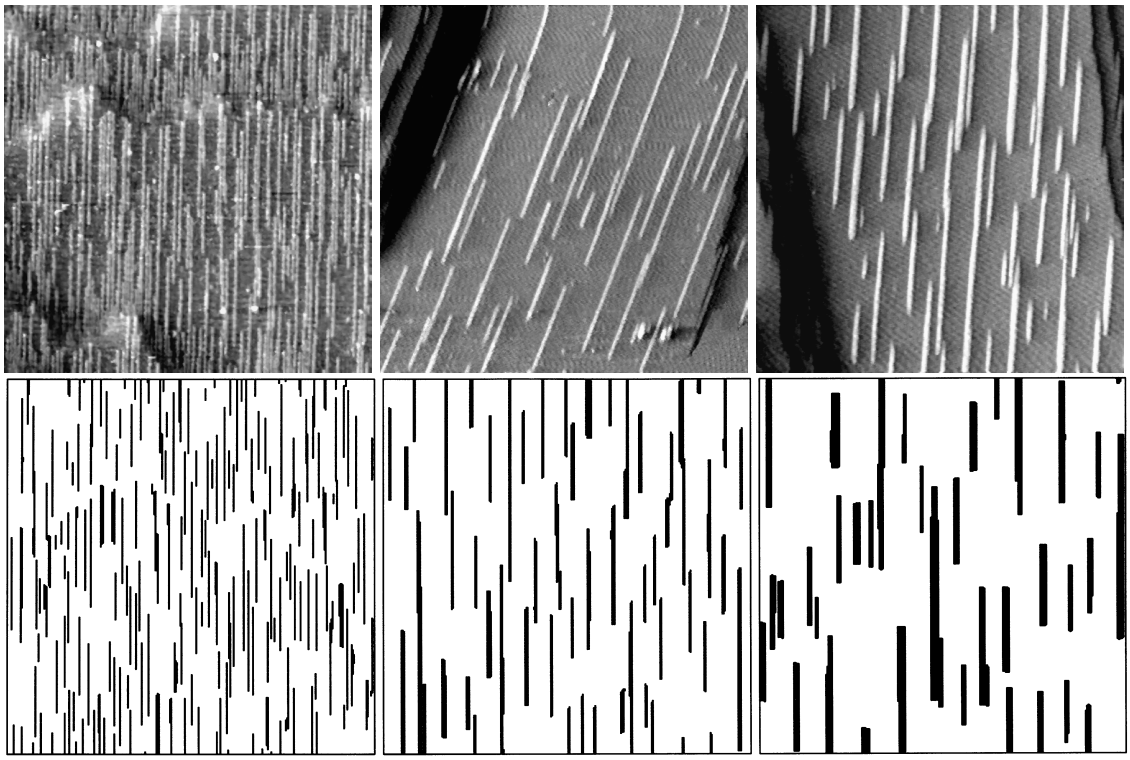

1. Top row: STM images (1200×1200 Å^2) of Cu islands on Pd(110) grown at 265K, 300K, and 320K (left to right). Bottom row: corresponding simulated film morphologies.

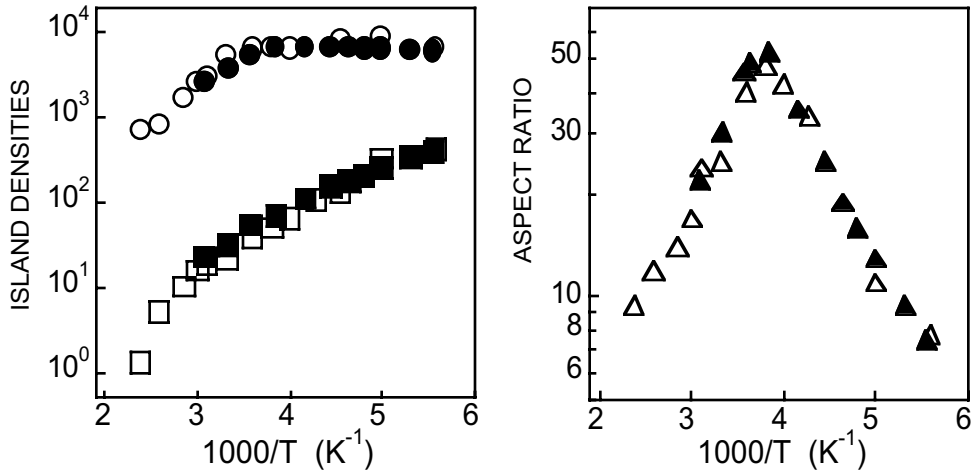

2. Arrhenius behavior of N_L(circles)=number of islands per unit length across the islands, N_A(squares)=number of islands per unit area, and α (triangles)=island aspect ratio. Open (solid) symbols are experimental (simulation) data. N_A=1 (N_L=1) corresponds to 1.7×10^{10} islands/cm^2 (420 islands/cm). At low T, the behavior of N_A is controlled by the terrace diffusion barriers. At higher T, it depends also on adatom-adatom bonding. The behavior of N_L depends on whether corner rounding is inoperative (at very low T), one-way (below 265K, where islands are chain-like), or two-way (above 265K). Below 265K, the rate at which adatoms impinge on the narrow island edges dominates the rate at which they can escape to the long edges. Only above 265K can island shapes equilibrate during growth. (Equilibrium shapes are also anisotropic in this system.)

ETCHING OF Si(001) WITH O_2

M.C. Bartelt, J.B. Hannon, N.C. Bartelt and G. Kellogg

Motivation:

Controversy exists concerning specific microscopic processes, and their rates, involved in the etching of Si surfaces with atomic or molecular oxygen, based on analysis of the species that evolve from the surface. Differences in surface structure and composition have been suggested as the source of disagreement, but experiments that are sufficiently simple to interpret, and can thus unequivocally address structure sensitivity issues in model systems, have not been reported. Modulated beam experiments have indicated that, at high surface temperatures, exposure of Si(001) to a low pressure of molecular oxygen produces volatile monoxide SiO, leading to a net removal of Si from the surface, at a temperature-dependent rate, without significant accumulation of oxygen on the surface. LEEM imaging *during* the initial stages of etching of our clean Si(001) surfaces reveals monatomic deep vacancy islands (pits) nucleated near the center of large terraces. These pits grow monotonically at a rate which clearly reflects differences in their local environment (e.g., the average density and size of neighboring pits). See Fig.1. We want to understand and characterize this environment dependence of pit growth, and ultimately identify the dominant atomic mechanisms, and measure the associated activation barriers and prefactors, for SiO formation, surface migration, and desorption. Very importantly, these parameters depend on the distribution of kinetically competitive Si-O bonding configurations, about which little is known with certainty.

Accomplishment:

We modeled this system with kinetic Monte Carlo simulations and diffusion equation analysis. The model incorporates creation of Si vacancies at random sites on the terrace, or adjacent to steps (following desorption of SiO, either from the adatom 'sea' or from active first-layer sites). Vacancies diffuse until they meet other diffusing vacancies, with which they irreversibly nucleate a pit, or an existing pit where they are also irreversibly incorporated leading to pit growth. For sufficiently high temperatures and low oxygen fluxes, new pit nucleation is rare compared to growth of existing pits. This model is applied to evolve pit distributions taken directly from experiment. With one parameter (the ratio of vacancy diffusion to vacancy creation, which we can measure independently from the scaling of the number density of pits with temperature and oxygen flux), we consistently reproduce the observed growth rate of pits in samples etched at temperatures ranging from 770 to 960°C. See Fig.2 for a typical match. We are in the process of testing every assumption in the model with additional experiments.

Significance:

Heterogeneous surface reactions affect some of the most important materials choices for the processing of semiconductor-based devices and catalytic metal surfaces. The primary motivation for studying the reaction of Si surfaces with oxygen has been the interest in ultra-thin SiO_2/Si interface for microelectronics applications. However, the kinetics of the transition from stable SiO_2 film formation to etching (and roughening) of the Si surface depend subtly on the local oxygen coverage and chemical and physical environment. This may provide unique control over the oxide structure and properties, but exploiting this requires the type of basic understanding that we are trying to develop about the various atomic-scale processes leading to the reaction. Studies of the reaction of Si with molecular oxygen are also particularly challenging (due to the low sticking coefficient), but the etching behavior differs significantly from that of the reaction with atomic oxygen to be potentially useful for investigation of molecular dissociation effects.

Publications:

Etching of the Si(001) surface with molecular oxygen, J.B. Hannon, M.C. Bartelt, N.C. Bartelt, and G.L. Kellogg, in preparation for submission to Phys. Rev. Lett..

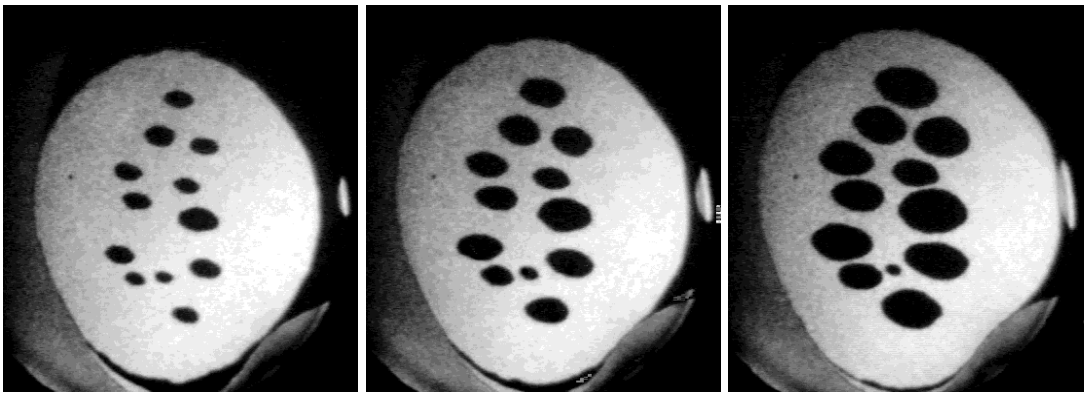

1. Dark-field LEEM images of the Si(001) surface, recorded at 840°C, during exposure to molecular oxygen. Dark "ellipses" are monatomic deep pits. Time increases from left to right.

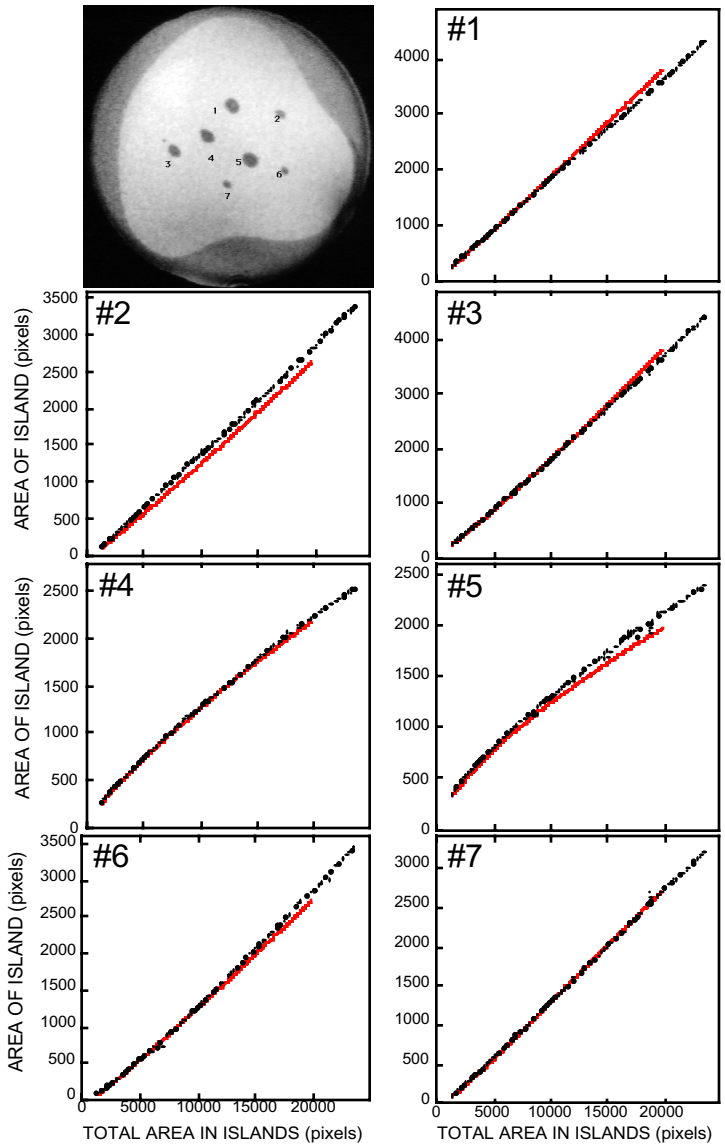

2. The growth of all seven vacancy islands on Si(001), for the sample shown in the first frame, during exposure to molecular oxygen at 960°C. Dark symbols are experimental data. Gray solid lines are results from our simulations.

Coarsening in Multicomponent, Multiphase Systems

J.J. Hoyt

Motivation:

The phenomenon of precipitate coarsening in binary alloys has been studied extensive for over 30 years. However, despite the fact that almost all commercial alloys are multicomponent and many are multiphase, very little theoretical or experimental work has been performed on these more complicated systems. The goal of the present research program is to extend existing theories of particle coarsening to the more general case of multicomponent, multiphase alloys and to illustrate new effects which can arise due to the extra compositional degrees of freedom.

Accomplishment:

The simplest treatment of coarsening is the mean field approximation of Lifshitz-Slyozov-Wagner (LSW). In the past year, we have applied mean field coarsening theory to the multiphase case and it has been shown that the rate constant describing the growth of the average size precipitate of any given phase is identical to an expression derived earlier for an single phase growing in a multicomponent system. In addition, the scaled particle size distribution for each phase is the same as the LSW form predicted for the binary case. The LSW theory is strictly valid only in the limit of a vanishingly small volume fraction of precipitate phase and several theoretical approaches have been employed to include the effects of a nonzero volume fraction. Recently, we have employed the diagrammatic method of Marqusee and Ross to a ternary system with two precipitate phases (β and γ). The analysis shows that, in general, the presence of one phase affects the growth rate of the second phase, but the "cross phase" effect depends on, among other variables, the topology of the ternary phase diagram. Figure 1 illustrates some of the essential ideas. The top drawing is the Gibbs triangle for the system showing the position and shape of the three phase triangle. It should be noted that both the γ and β phases are competing for solute species 1 whereas only the γ particles require species 2 from the matrix. The rate constant normalized by the mean field value as a function of volume fraction (where the total volume fraction of $\beta+\gamma$ is 10%) is shown in the bottom plot. Two different results are shown; the case where the diffusion constant of species 1 equals that of species 2 and the case where D_2 is a factor of 10 larger than D_1. The variation with volume fraction and relative diffusivities illustrates the complex interplay between the growth of the two phases.

Significance:

The low volume fraction coarsening theory provides, for the first time, a quantitative description of the growth of more than one precipitate phase in a multicomponent alloy.

Publications:

J. J. Hoyt, "A Mean Field Description of the Kinetics of Precipitate Free Zone Formation", Scripta Mater., 37, 2033 (1997).

J. J. Hoyt and J. E. Morral, "Coarsening in Multicomponent, Multiphase Systems I, the Mean Field Limit", submitted to Acta Mater., (1997).

J. J. Hoyt, "Coarsening in Multicomponent, Multiphase Systems II, a Low Volume Fraction Expansion", in prep.

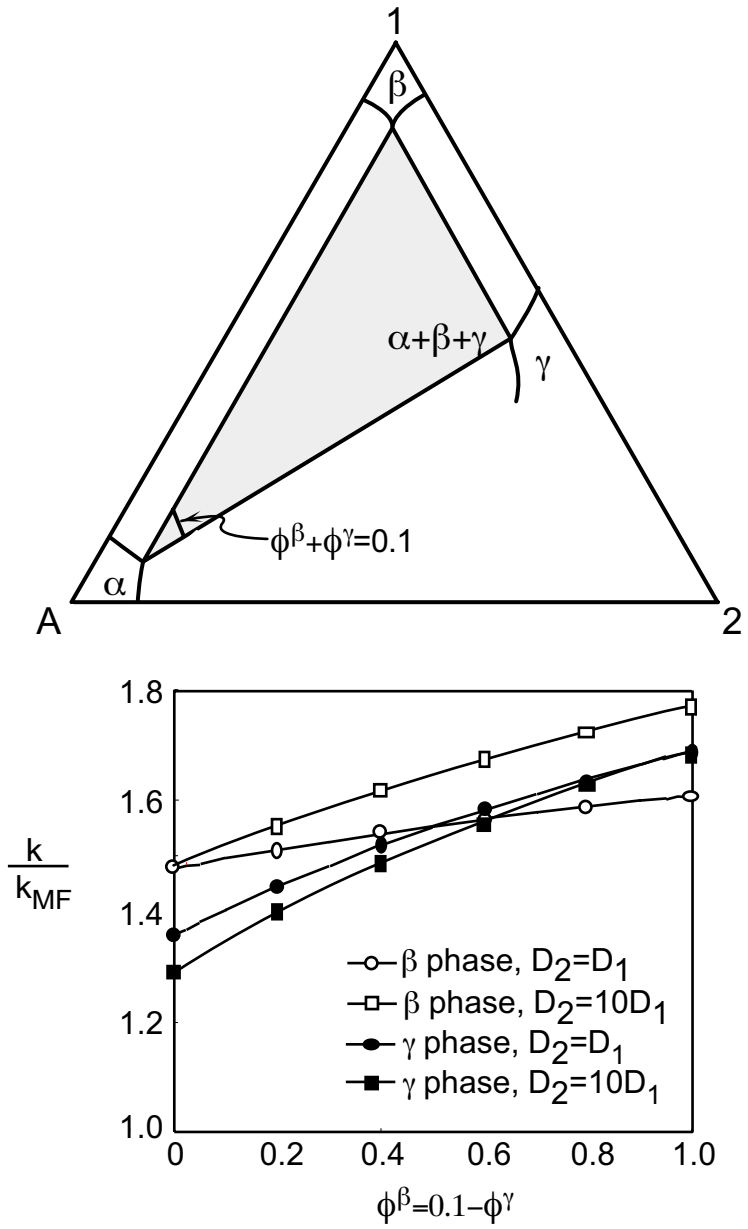

Fig. 1. Top, Gibbs triangle for a ternary three phase coarsening system. Bottom, rate constant vs. volume fraction dependence for two values of the relative diffusivities.

First-Principles Calculations of Interfacial Thermodynamic Properties in Alloys

M. Asta, A.A. Quong and S.M. Foiles

Motivation:

The thermodynamic properties of interfaces play a critical role in dictating mechanical properties and microstructural evolution in materials. Despite their importance, reliable values for interfacial free energies are often unavailable, due to the extreme difficulty associated with their direct experimental measurement. In alloys interfaces are generally not compositionally abrupt at finite temperature. Interfacial free energies are minimized through the creation of diffuse composition profiles. The width of these composition profiles, as well as the composition and temperature-dependences of interfacial free energies, are controlled by a subtle balance between energetic and entropic factors. The calculation of interfacial free energies in alloys requires a technique which allows both contributions to be computed with comparable high accuracy. We have employed first-principles-based cluster-expansion techniques to solve this problem.

Accomplishment:

We have successfully applied first-principles-based techniques to the calculation of a wide variety of interfacial thermodynamic properties in substitutional alloys. As an example, in Fig. 1 we plot calculated free energies for {111} and {100} antiphase boundaries (APBs) in γ-TiAl. The filled circles represent first-principles-calculated APB energies obtained at zero Kelvin for equiatomic TiAl alloys. The filled diamond and square represent APB energies measured experimentally (Hug et al., 1988 and Stucke et al., 1995) for off-stoichiometric samples which were deformed at T=873 K. The large difference between the experimentally-measured values and the calculated results at zero Kelvin has been a topic of considerable interest in the intermetallic literature. Our calculations demonstrate that this discrepancy can be attributed to the effect of composition and temperature upon the values of the APB free energies. The open circles in Fig. 1 are first-principles results calculated as a function of composition at T=873 K. At finite temperature, compositional rearrangements within the vicinity of the APBs gives rise to a lowering of the APB free energy which is enhanced for off-stoichiometric compositions. Our results for Al-rich APB free energies at T=873 K agree exceptionally well with experimental measurements. Similar calculations to those highlighted in Fig. 1 have been preforemed for coherent heterophase interfaces in Al-Ag and Al-Sc alloys.

Significance:

The techniques developed in this work can be used to enhance our fundamental uncerstanding of interfacial thermodynamic properties, while providing values of interfacial free energies required in larger-length-scale modeling of microstructure and mechanical properties. Future work in the topic of alloy interfaces will involve: (i) assessment of the importance of nonconfigurational entropy contributions, (ii) the study of solid-liquid interfacial free energies in alloys, and (iii) first-principles studies of impurity segregation to alloy interfaces.

Publications:

- M. Asta and A. A. Quong, "The concentration and temperature dependences of antiphase-boundary energetics in γ-TiAl: a first-principles study," Phil. Mag. Letters **76**, 331 (1997).
- M. Asta, S. M. Foiles and A. A. Quong, "First-principles calculations of bulk and interfacial thermodynamic properties for fcc-based Al-Sc alloys," Phys. Rev. B (in press).

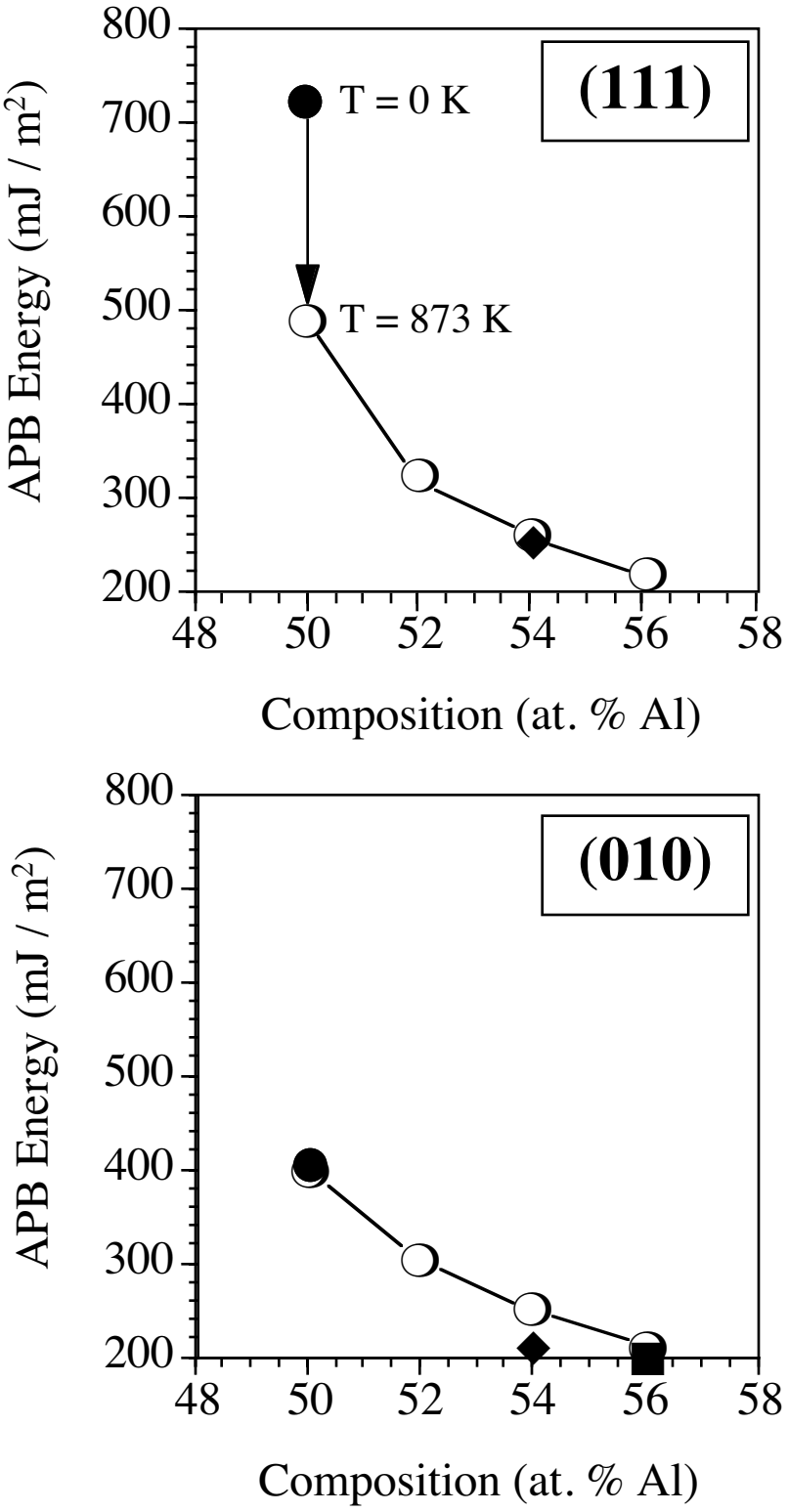

Fig. 1: Calculated and measured APB energies for {010} and {111} APBs in g-TiAl. Filled and open circles represent calculated results at T=0 K and T=873 K, respectively. Filled diamond and square symbols represent measured results by Hug et al. and Stucke et al., respectively, for samples deformed at T=873 K.

Theoretical and Experimental Studies of Ordering in Ternary Alloys

M. Asta, J.J. Hoyt and A.A. Quong

Motivation:

In long-range-ordered alloy phases each atomic species preferentially occupies different sublattice sites. The nature of the site preferences in ordered alloys has important consequences for phase stability and a wide variety of physical properties. Experimentally, site occupancies in a binary alloy can be determined from a single diffraction experiment. In a ternary system with two sublattices there exists two independent order parameters and the determination of both requires a combination of at least two diffraction techniques where the scattering factors of each species in the alloy is substantially different in each experiment. Theoretically, the prediction of site occupancies in a ternary (A-B-C) alloy is complicated by the fact that each of the A-B, B-C and A-C sets of interactions must be described with comparable accuracy. We have applied the combination of neutron and x-ray diffraction to measure, for the first time, the two long range order parameters in Cu_2AlMn in the vicinity of the BCC→*B*2 transition. The qualitative nature of the site preferences in this system have been reproduced by first-principles calculations performed with two independent and complimentary approaches.

Accomplishment:

In-situ high temperature x-ray and neutron powder diffraction experiments, both performed at the Oak Ridge National Lab user facilities, were performed for the *B*2 phase of Cu_2AlMn at seven temperatures just below the BCC→*B*2 critical temperature of 1002 K. A Reitveld refinement of the powder patterns showed that the Al atoms were enriched on the Al+Mn sublattice, whereas Mn showed only a very weak preference for the same sublattice. The results are represented in Fig. 1. The measured compositions for each sublattice in the B2 structure are plotted as solid circles on a Gibbs triangle, connected by the thin solid line. The rotation of this solid line away from the dashed line illustrates the measured Al enrichment. This Al enhancement is well reproduced by first-principles calculations performed with two independent approaches. In the first, the KKR-CPA method is employed to calculate the polarization of the critical concentration wave just above the transition temperature. The KKR-CPA predicts that the ratios of the concentrations on the two *B*2 sublattices should correspond to a line with the slope given by the thick solid line in Fig. 1. This line is rotated away from the dashed line in the same sense as the experimental measurements, reproducing the Al-enhancement on the Al+Mn sublattice. The open symbols in Fig. 1 were obtained by the LMTO-CVM first-principles computational approach. These symbols were obtained as a function of temperature below the BCC → *B*2 transition and also reproduce the measured Al enhancement.

Significance:

This research has demonstrated how order-disorder transitions and site occupancies in ternary alloys can be studied both experimentally, using a combination of diffraction techniques, and theoretically, using two independent first-principles approaches. Future work will couple experimental work and calculations for other ternary systems including Al-Ti-Nb and Al-Ti-V.

Publications:

∑ R. P. McCormack, M. Asta, J. J. Hoyt, B. C. Chakoumakos, S. T. Misture, J. D. Althoff and D. D. Johnson, "Experimental and Theoretical Investigations of Order-Disorder in Cu_2AlMn", Comp. Mater. Sci. **8**, 39 (1997).

∑ M. Asta, D. D. Johnson, J. D. Althoff and A. A. Quong, "First-Principles Study of Site Occupancies in Ternary *B*2 Ti-Al-Nb Alloys," in preparation.

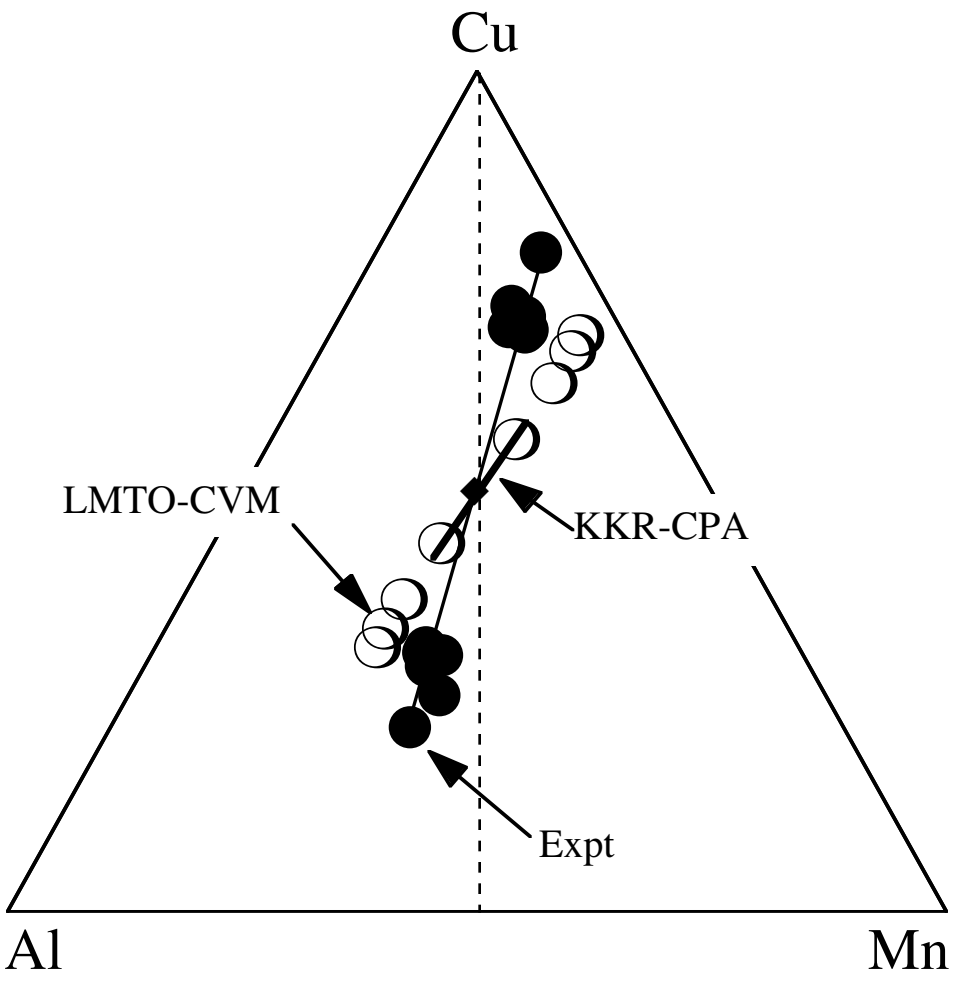

Fig. 1: Calculated and measured sublattice occupancies for *B*2 Cu_2AlMn.

New Process for Synthesizing Thick Films of Cubic Boron Nitride

K.F. McCarty and D.L. Medlin

Motivation:

Cubic boron nitride possesses physical properties, including hardness and thermal conductivity, that are comparable to diamond. Unfortunately, cBN films have been limited to about 100-200 nm in thickness because high residual stresses cause delamination of thicker films.

Accomplishment:

By first understanding how cBN forms in energetic deposition, we have developed a new hybrid process for synthesizing thick films of cubic boron nitride (cBN). The process combines sputtering of a boron carbide target, nitrogen ions, and growth on a high-temperature substrate. The combination of low-energy ions (about 100 eV) and high temperature greatly reduces the residual film stress that has plagued other growth techniques. Using nanoindentation, the films were found to be extremely hard, having hardness values of about 60 GPa. This is slightly harder than bulk cBN and only diamond is harder. Using transmission electron microscopy, we found a novel orientation relationship in the films -- the close-packed, {111} planes of the cBN crystallites are strongly aligned with the basal, (0002) planes of the graphitic boron nitride that forms in the initial stages of film growth. We have established that the graphitic BN texture results from plastic deformation and the cBN texture comes directly from the growth mechanism in which graphitic BN is transformed to cBN.

Significance:

Our new hybrid process that produces thick, low-stress films, is a significant breakthrough. We have used the resulting thick films to evaluate physical properties such as hardness. Previous hardness measurements of thin cBN films were limited by substrate effects and gave ambiguous results. Our measurements of the thick cBN films are largely free of substrate effects and unambiguously (and encouragingly) show that the films are as hard as bulk material. Finally, this work provides direct insight into how cBN nucleates and grows in these ion-assisted processes.

Publications:

P. B. Mirkarimi, K. F. McCarty, and D. L. Medlin, "Review of Advances in Cubic Boron Nitride Synthesis," Mater. Sci. Engin. Reports, accepted (1998).

K. F. McCarty and D. L. Medlin, "How Plastic Deformation can Produce Texture in Graphitic Films of Boron Nitride, Carbon Nitride, and Carbon," Diamond Relat. Mater. **6** 1219 (1997).

P. B. Mirkarimi, D. L. Medlin, K. F. McCarty, D. C. Dibble, W. M. Clift, J. A. Knapp, and J. C. Barbour, "The Synthesis, Characterization, and Mechanical Properties of Thick, Ultrahard Cubic Boron Nitride Films Deposited by Ion-Assisted Sputtering," J. Appl. Phys., **82** 1617 (1997).

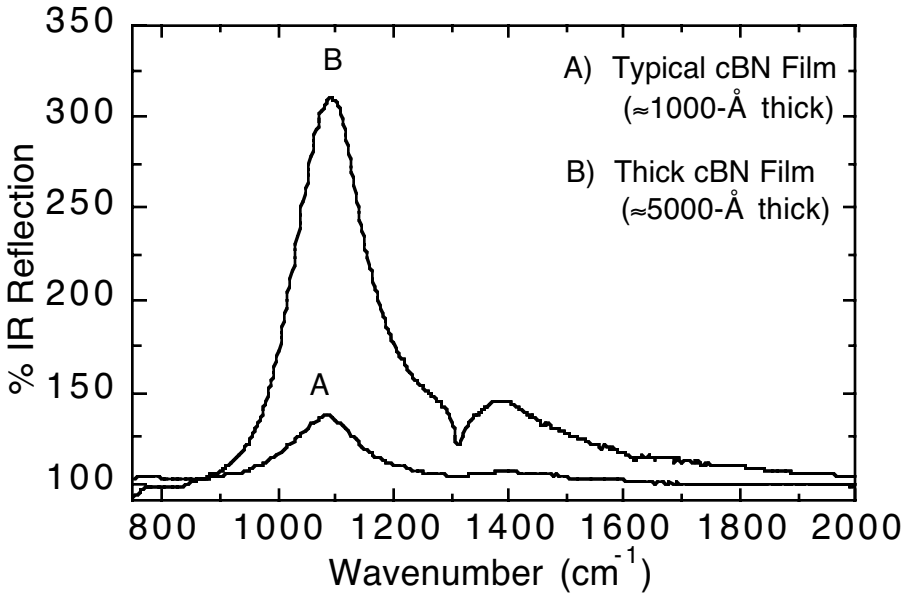

Fig. 1. Infrared spectra of A) a typical (1000-Å-thick) cBN film, and B) a 5000-Å-thick film produced by the new process.

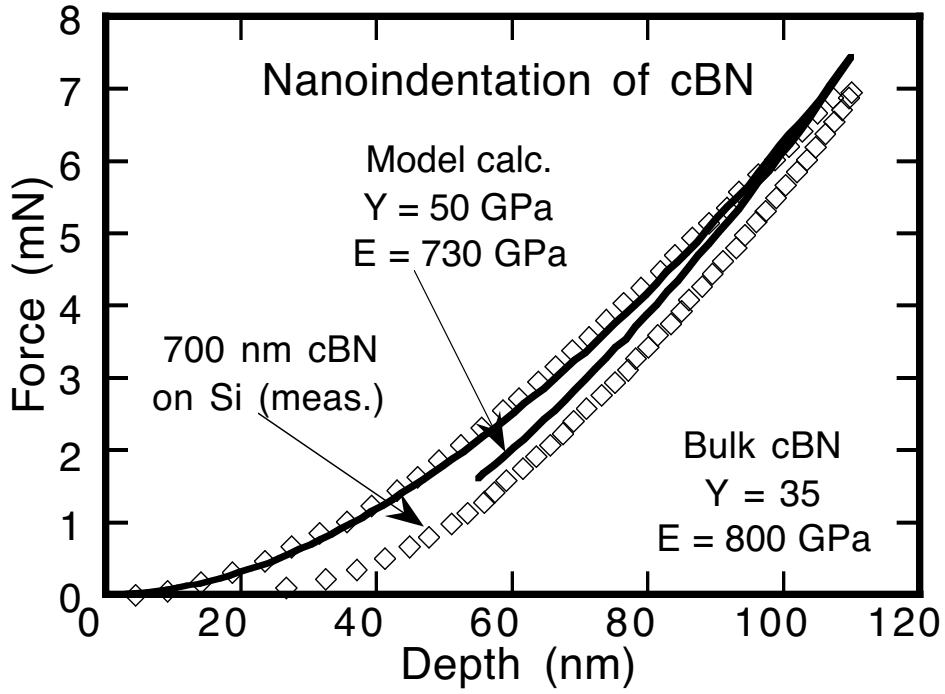

Fig. 2. Indentation loading (upper squares) and unloading (lower squares) curves for a 7000-Å-thick cBN film. Analysis shows the film (60 GPa hardness) to be as hard as bulk cBN. Finite-element analysis of the indentation (solid lines) gives a film modulus of 730 GPa, compared to 800 GPa for bulk cBN.

First Principles Calculations of Structure of Nucleating Heteroepitaxial Thin Films

J.C. Hamilton and R. Stumpf

Motivation:

The morphology of heteroepitaxial thin films is largely determined by the nucleation of islands and the development of dislocations and other structures which relieve strain, but often introduce undesired defects into films. Prediction of these structures formed during early growth involves a complex interplay of kinetics and energetics. Although accurate energetic calculations are required in order to predict film properties, the extension of these results to the large structures occurring during heteroepitaxial film nucleation is challenging because of the large number of atoms involved. We have combined first principles calculations with a double sine Gordon model in order to solve this problem.

Accomplishment:

We have bridged the gap between highly accurate first principles calculations, and much larger scale structures involving dislocations. The system chosen for study was the formation of Ag films on Pt(111) surfaces. Experimental data for this system shows an unusual pattern of very narrow hcp domains separated by very wide fcc domains. The experiments also measure the quantitative relationship between dislocation formation and island size. Using a double sine Gordon model with parameters derived from first principles, quantitative agreement has been obtained between our theory and all of the experimental observations. Figure 1 shows the result of our calculation for a submonolayer film. The ratio of the domain widths, hcp:fcc::1:3.5, is in excellent agreement with the experiment. We find that the very wide fcc domain widths occur because this particular overlayer system is remarkably close to the phase transition between a dislocated and a pseudomorphic phase. This conclusion is in quantitative agreement with the fact that the structure changes from dislocated to pseudomorphic as the coverage increases from submonolayer to above a monolayer. Figure 2 shows the measured and calculated probability of dislocation incorporation in an island as a function of island size assuming thermal equilibrium between dislocated and pseudomorphic islands.

Significance:

This work allows for the first time a precise understanding of the reasons why relative widths of fcc and hcp domains vary so widely in different dislocation systems (and why they are so dramatically different for Ag on Pt(111)). The fundamental reason for very different widths of the two domains is the extreme proximity of this system to the phase transition. Understanding this phenomena is key to obtaining quantitative information regarding stacking fault energies from experimental observations of these overlayer dislocation patterns. In particular it is shown that knowledge of the Ag-Ag interaction in the overlayer is just as important to determining the relative domain widths as is the stacking fault energy. Finally this work represents the first quantitative prediction of a morphological change in island structure as a function of island size. It is found here that near equilibrium occurs between dislocated and pseudomorphic islands, allowing prediction of dislocation formation from the relative energies of the two different structures.

Publications:

Double Sine Gordon Model of Commensurate-Incommensurate Phase Transition of Ag on Pt(111), in preparation for submission to Physical Review Letters, J. C. Hamilton, N. Bartelt, R. R. Stumpf, Harald Brune, G. Kresse, Jurgen Hafner

Figures

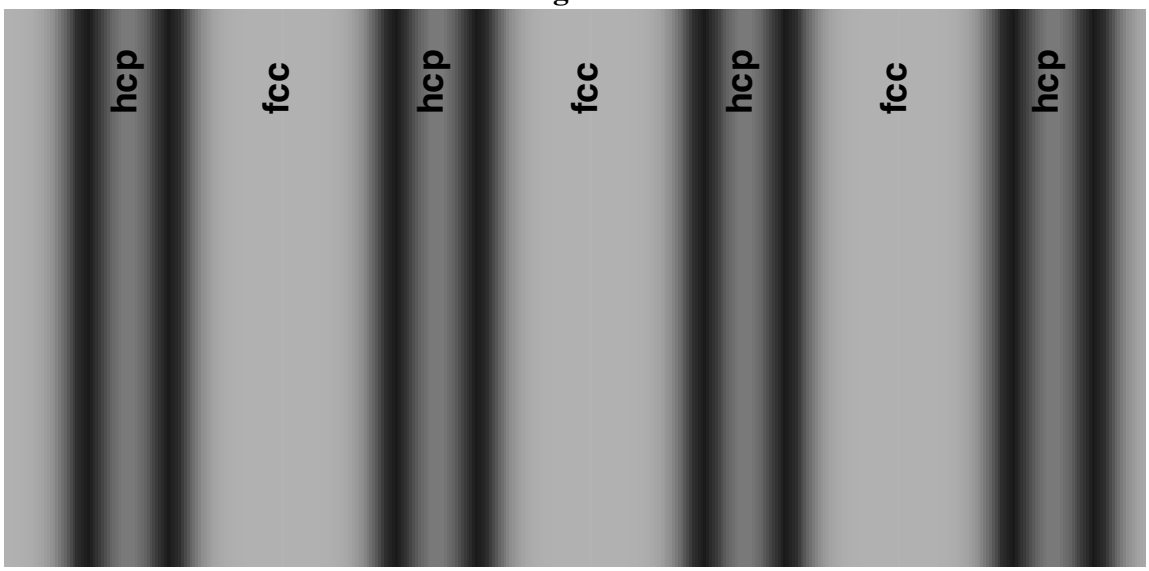

1) Calculated dislocation structure for submonolayer silver on platinum (111). The structure has domains with fcc and hcp stacking separated by Shockley partial dislocations. The very wide fcc domains relative to the narrow hcp domains occur because this system is extremely close to the phase transition to the pseudomorphic phase. This structure calculated from first principles is in excellent agreement with experiment.

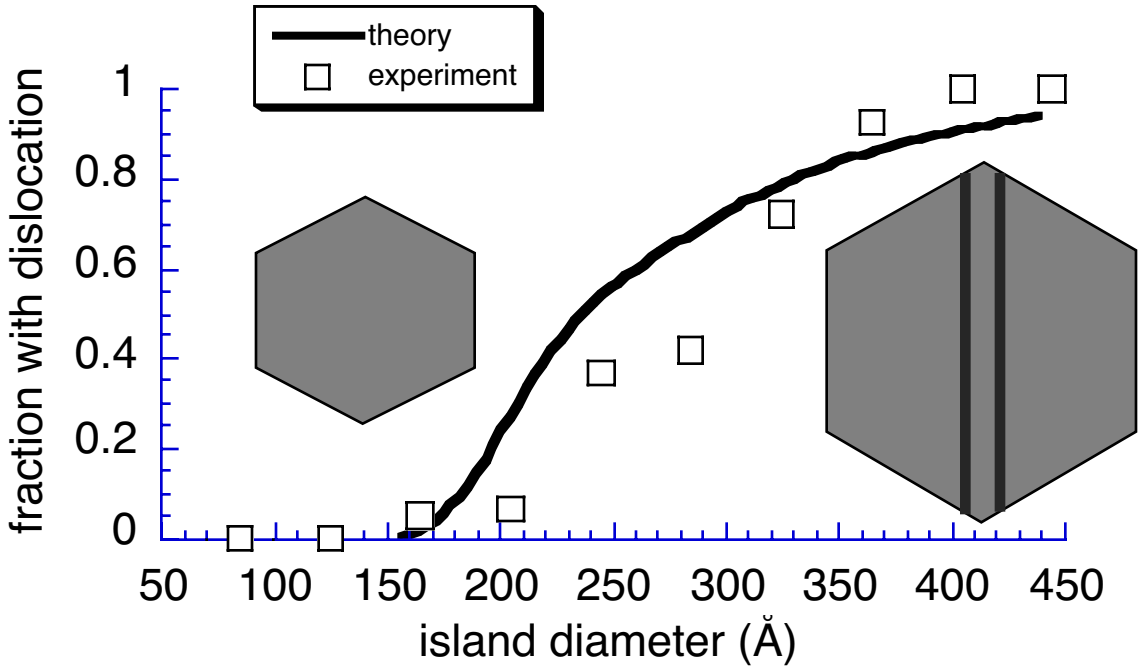

2) Experimental and theoretical results for probability of dislocation inclusion as a function of island size. Experimental data is shown as open squares, theory is solid line. Hexagons represent schematics of islands with and without dislocations

Atomistic processes in the chemical reactivity of strained metal films

J. de la Figuera, A.K. Schmid, N.C. Bartelt, J. Hrbek and R.Q. Hwang

Motivation:

The unique chemical properties of metal films form the basis of technologies ranging from protective coatings to catalysis. Strain is a primary reason of these novel properties although little understanding of how this occurs presently exists. We have used scanning tunneling microscopy to investigate the response of the strained metal film to exposure to reactive gases such as oxygen and sulfur.

Accomplishment:

Figure 1a - d shows a sequence of STM images of a 2 layer Cu film on Ru(0001) during exposure to oxygen. Dislocations present in the film are altered by reaction with oxygen. Edge dislocations are generated by connecting two partial dislocations (stripes). This reaction is due to the relaxation of stress in the film due to its interaction with oxygen leading to a higher density of edge dislocations. The dislocations enhance the reactivity of the film several orders of magnitude as compared to bulk Cu. This process is more general in that an identical process is found with exposure to sulfur. These measurements point to the atomistic processes related to corrosion and the enhanced reactivity of strained metal films.

Significance:

This process is the initial step to the corrosion of the film by oxygen. The structural changes in the film, i.e., the higher density of dislocations is also important in defining the mechanical properties of the film. Thus, the link between chemical reaction processes and mechanical properties are being investigated.

Publications:

Multiplication of Edge Dislocations in Strained Metal Films under Oxygen and Sulfur Exposure, J. de la Figuera, K. Pohl, A.K. Schmid, N.C. Bartelt, J. Hrbek and R.Q. Hwang, in preparation.

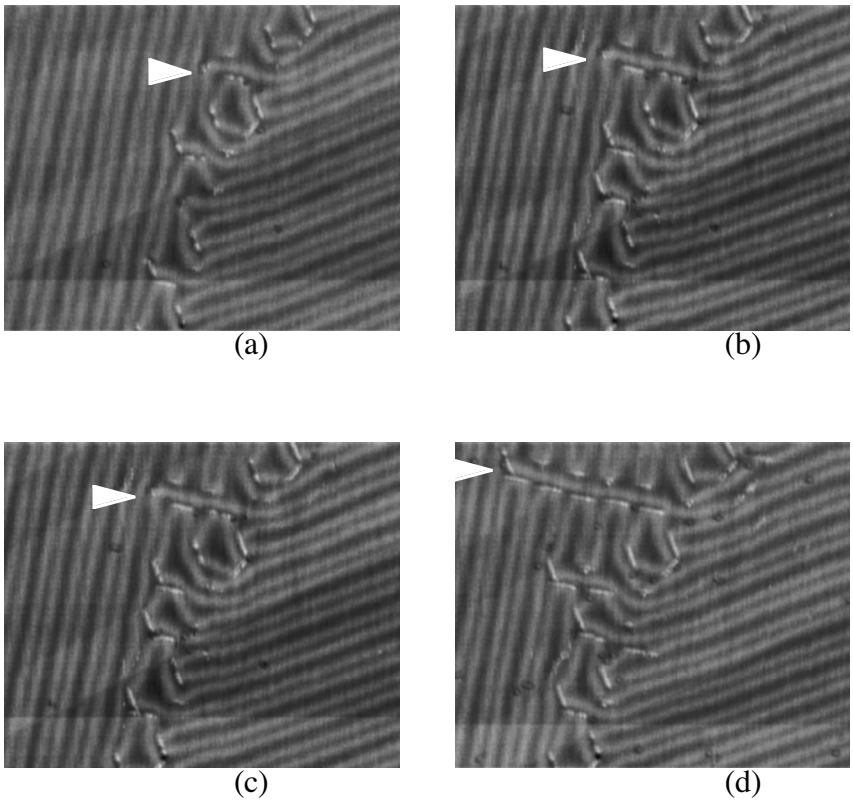

Fig. 1a-d: A sequence of 75nm X 60nm STM images of a 2 atomic layer film of Cu on Ru(0001) under exposure to oxygen. The bright stripes are partial dislocations, and where they meet, edge dislocations are formed. The oxygen systematically multiplies the edge dislocations by linking partials.